Energy Engineering

Tech Science Press

http://doi.org/10.32604/ee.2026.083133

ARTICLE

An Improved VSG Control Strategy for Wind Storage Combined System Oriented to Active Frequency Support

Ruanming Huang[1], Yuchen Qi[1], Yaoliang Zhu[1], Chen Qian[1], Haojie Li[2,*] and Bing Wang[2]

[1]State Grid Shanghai Municipal Electric Power Company, Shanghai, China
[2]College of Artificial Intelligence and Automation, Hohai University, Nanjing, China
[*]Corresponding Author: Haojie Li. Email: lhj16638275321@163.com

Received: 30 March 2026; Accepted: 03 June 2026; Published: 30 August 2026

ABSTRACT: With the continuous expansion of installed capacity of renewable energy represented by wind power, modern power systems are increasingly characterized by high penetration of power electronics. This trend leads to reduced system inertia and compromised disturbance resilience, posing prominent challenges to frequency stability. Mainstream wind turbines operating in maximum power point tracking (MPPT) mode typically lack effective responses to system frequency fluctuations. Although conventional fixed-parameter virtual synchronous generator (VSG) technology can provide inertial support, it struggles to balance dynamic response speed and operational stability under variable operating conditions. To address these issues, this paper proposes an adaptive inertia and damping integrated VSG control strategy based on the synergy of fuzzy logic and particle swarm optimization (PSO), which is applied to grid-connected wind power systems with DC-side energy storage. Firstly, a combined wind-storage system model is established, integrating wind turbines, energy storage units, and converters. The overall control architecture is defined, including machine-side vector control, energy storage-based DC bus voltage regulation, and grid-side VSG control. Secondly, a small-signal model of the VSG is developed, and the root locus method is employed to analyze the influence of key parameters on system stability. Subsequently, a hierarchical parameter coordination strategy is developed, in which the virtual inertia is adjusted online by fuzzy logic to provide fast inertial support, while the damping coefficient is optimized offline by PSO to improve oscillation damping and steady-state recovery. Compared with adaptive VSG methods with simultaneous multi-parameter variation, the proposed online-offline coordinated design reduces the coupling risk between virtual inertia and damping coefficient and improves the dynamic frequency support capability of the wind-storage combined system. Finally, a simulation model of the wind-storage system is built on the MATLAB/Simulink platform. Simulation results demonstrate that, compared with traditional control strategies, the proposed method can significantly reduce frequency deviation and regulation time under conditions of sudden load changes and wind speed fluctuations. It effectively enhances the system's active frequency support capability while maintaining the stability of the DC bus voltage, verifying its superior performance and engineering application potential. Furthermore, the proposed strategy provides a feasible active frequency support solution for wind-storage combined systems in high-renewable power grids, and its future applicability can be further verified through hardware-in-the-loop tests and experimental implementation under practical operating conditions.

KEYWORDS: Wind-storage system; VSG control; fuzzy logic; particle swarm optimization; active frequency support; small-signal model

1 Introduction

With the in-depth advancement of the "carbon neutrality" strategy, the installed capacity of renewable energy sources such as wind power has been continuously expanding. Consequently, modern power systems are gradually presenting the "dual-high" characteristics, i.e., a high proportion of renewable energy penetration and a high proportion of power electronic equipment integration [1]. However, mainstream variable-speed wind turbines typically operate in the maximum power point tracking (MPPT) mode, where their rotational speed is decoupled from the grid frequency. Unlike traditional synchronous generators, they are unable to provide inherent physical inertia support to the power system [2]. As the penetration ratio of synchronous generators decreases, the equivalent inertia of the system is significantly reduced, resulting in weakened disturbance resilience. When the power system experiences sudden load changes or power fluctuations on the generation side, the rate of frequency change (RoCoF) increases sharply. This not only raises the risk of frequency exceeding the allowable limit but may also trigger severe accidents such as large-scale blackouts in extreme cases [3].

To address the challenges of insufficient system inertia and compromised frequency stability, virtual synchronous generator (VSG) technology has emerged as a promising solution. Zhong et al. [4] first established the theoretical framework of VSG, proposing that by introducing virtual inertia $\mathcal{J}$ and damping coefficient D, grid-connected inverters can be endowed with external characteristics similar to those of synchronous generators, thereby enabling autonomous frequency support. In the field of wind power applications, Reference [5] verified that the VSG-based wind turbine control strategy can convert system frequency fluctuations into DC voltage variations, and further utilize the rotor kinetic energy of wind turbines to provide grid support. As such, VSG has become a key technology for enhancing the grid compatibility of renewable energy in modern power systems [6]. However, traditional VSG strategies typically adopt fixed control parameters, which exhibit inherent limitations under complex and variable operating conditions: a larger virtual inertia J can effectively suppress the rate of frequency change (RoCoF), but it may introduce phase lag, prolong the dynamic regulation time, and lead to power overshoot; conversely, a larger damping coefficient D helps mitigate system oscillations, yet it tends to increase steady-state frequency deviation. Regarding the parameter tuning issue, Reference [7] conducted an in-depth analysis of the interactive effects of J and D on transient responses, pointing out that flexible parameter adjustment is crucial for optimizing system performance. Reference [8] further revealed the coupling mechanism between virtual inertia and virtual damping, and proposed a coordinated control method based on the system oscillation mode. To achieve dynamic parameter optimization, existing research primarily falls into two categories: adaptive control and intelligent algorithm-based optimization. In terms of adaptive control, some scholars [9] introduced fuzzy logic, leveraging its advantage in handling nonlinear problems to adjust virtual inertia online according to frequency deviation and its rate of change, which effectively improves the system transient response. Reference [10] also proposed an improved adaptive inertia control technique, significantly enhancing the frequency regulation capability of microgrids. In the field of intelligent algorithms, particle swarm optimization (PSO) and its improved variants have gained widespread attention due to their superior global optimization capabilities. Reference [11] proposed an adaptive VSG parameter tuning strategy based on an particle swarm optimization (PSO) algorithm, addressing the low accuracy issue of traditional empirical parameter setting methods. The research work in References [12,13] verified the convergence and effectiveness of improved PSO algorithms in multi-objective parameter optimization tasks. Furthermore, Reference [14] explored frequency control optimization based on meta-heuristic algorithms, which further enriches the technical pathway for VSG parameter tuning. Reference [15] combined adaptive parameter adjustment with optimization algorithms, achieving favorable results in improving transient frequency response performance. Despite the significant progress made in the aforementioned studies on VSG parameter optimization, most of them focus on ideal DC power sources or rely on a single control method, often neglecting the physical constraints imposed by the actual operating states of wind turbines on their frequency support capabilities. When wind turbines operate in maximum power point tracking (MPPT) mode, they lack sufficient reserve power to provide continuous inertial support and thus must rely on energy storage units for auxiliary regulation. Zhang et al. [16] conducted in-depth research on the virtual inertia demand of wind-storage combined systems, pointing out that the reasonable allocation of wind and storage energy is a prerequisite for achieving safe and effective frequency support. For DC microgrid scenarios, References [17,18] further proposed multi-stage coordinated speed regulation technologies, which address the frequency support problem of wind-storage systems under varying wind speed conditions. However, excessive reliance on energy storage units not only significantly increases the system investment and operation & maintenance costs, but is also constrained by the physical and economic limits of energy storage capacity. Therefore, how to fully exploit the active frequency support potential of wind turbines (or offshore wind farm clusters) and realize the dynamic optimization of virtual inertia and damping parameters under complex and variable wind conditions has become a research hotspot for improving the frequency stability of power systems [19]. Since the electromechanical energy conversion process of wind farms features strong nonlinearity and multi-time-scale dynamic characteristics [20], single intelligent optimization algorithms (e.g., conventional particle swarm optimization) often suffer from problems such as easy trapping in local optima or slow convergence when dealing with such complex operating conditions. Fuzzy logic control, despite its strong robustness to nonlinear systems, relies excessively on expert experience for rule base establishment, making it difficult to achieve optimal parameter matching globally. To this end, the deep integration of fuzzy adaptive control and advanced heuristic algorithms (e.g., PSO) provides a superior technical approach for the real-time dynamic optimization of key VSG parameters (virtual inertia J and damping coefficient D) [21].

In recent years, hybrid artificial intelligence (AI)-based methods have been increasingly applied to renewable energy systems, including power prediction, energy storage optimization, parameter tuning, and coordinated control. Compared with single-model approaches, hybrid AI methods can integrate the advantages of deep learning, ensemble learning, evolutionary optimization, and physical mechanism constraints, thereby improving prediction accuracy, optimization efficiency, and control robustness under nonlinear and uncertain operating conditions [22]. For example, Neshat et al. proposed a MetaWave Learner for wave farm power output prediction, in which convolutional neural network-based surrogate models were combined with an optimized extreme gradient boosting meta-learner. Their results demonstrated that hybrid deep ensemble learning can improve the robustness and accuracy of renewable power prediction under different marine energy scenarios [23]. Parsa reviewed recent developments in physics-informed machine learning for renewable energy systems and pointed out that combining data-driven models with physical laws can improve model interpretability, reliability, and generalization capability in wind, solar, ocean, and hybrid renewable energy systems [24].

Building on the aforementioned literature review, this paper proposes an improved VSG control strategy with online adaptive virtual inertia and offline optimized damping coefficient for a grid-connected wind-storage combined system. The novelty of this paper does not lie in a simple combination of fuzzy logic and PSO, but in the hierarchical coordination of DC-side energy storage support and grid-side VSG frequency regulation. Specifically, fuzzy logic is used to adjust the virtual inertia online according to frequency deviation and its rate of change, while PSO is employed to optimize the damping coefficient offline based on the ITAE index. This online-offline coordinated parameter design aims to improve the inertial response during the initial stage of disturbances and enhance oscillation damping during the recovery stage, while reducing the coupling risk caused by simultaneous online variation of both virtual inertia and damping coefficient.

The main contributions of this paper are summarized as follows:

(1) A wind-storage combined VSG control framework is established by integrating machine-side vector control, energy-storage-based DC bus voltage regulation, and grid-side VSG frequency support. In this framework, the energy storage unit not only maintains the DC bus voltage stability but also provides fast power support for active frequency regulation.

(2) An online-offline coordinated parameter design method is proposed. Different from conventional fixed-parameter VSG strategies or adaptive VSG methods with simultaneous multi-parameter variation, the proposed method adjusts the virtual inertia online by fuzzy logic and optimizes the damping coefficient offline by PSO, thereby improving transient frequency support while reducing parameter coupling.

(3) A small-signal model and root locus analysis are used to reveal the influence of virtual inertia and damping coefficient on system stability. On this basis, the ITAE index is introduced to guide the damping coefficient optimization, so that the optimized parameter is directly associated with the dynamic frequency response.

(4) Simulation studies under bidirectional load disturbances and wind speed variations are carried out to verify the effectiveness of the proposed strategy. In addition, a GWO-based co-optimized VSG strategy is introduced as an advanced comparison method to further evaluate the performance of the proposed PSO-based damping optimization.

2 System Structure Modeling

The wind-storage power generation system proposed in this paper, based on the virtual synchronous generator (VSG) control strategy, is composed of a permanent magnet synchronous generator (PMSG), a lithium-ion battery energy storage system, an AC/DC converter, a load, a DC/AC converter, and a DC bus. Its topological structure is illustrated in Fig. 1. In the system, P_w denotes the power generated by the wind turbine, P_m represents the mechanical power input to the generator, P_e stands for the electromagnetic power output by the generator, and P_s denotes the power exchanged between the wind turbine unit and the energy storage battery.

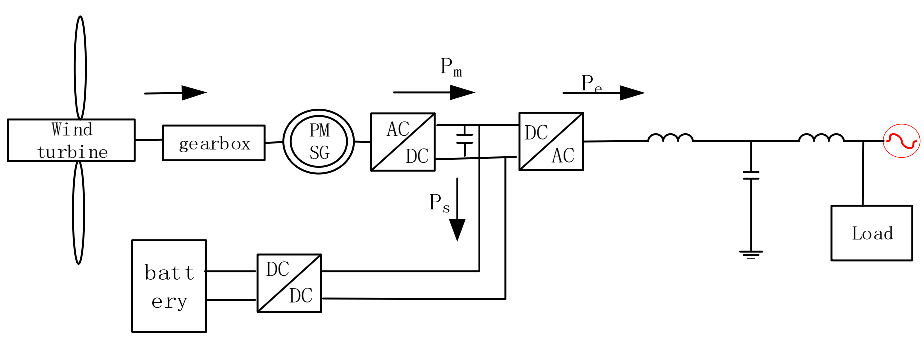

Figure 1: Structure block diagram of wind-storage power generation system.

The machine-side converter of the wind turbine adopts vector control, the energy storage system employs double-loop control, and the grid-side converter is configured with VSG control. The wind turbine and energy storage device are connected to the DC bus via an AC/DC converter and a DC/DC converter, respectively.

In the steady-state operation of the system, the wind turbine operates in the MPPT mode, while the VSG control does not participate in grid frequency regulation. The energy storage device remains in a standby state to conserve energy and provide backup power. When the system is subjected to disturbances, the wind-storage power generation system activates the VSG control strategy to mimic the frequency response characteristics of synchronous generators. Specifically, it adjusts the active power output of the wind-storage system to participate in grid frequency regulation; meanwhile, the energy storage device discharges to provide transient compensation for the system's active power deficit and maintain the stability of the DC bus voltage.

To further clarify the working principle of the wind-storage combined system, Fig. 2 illustrates the overall signal flow of the proposed adaptive VSG control strategy. The system consists of three coordinated layers: the machine-side layer, the DC-link/storage layer, and the grid-side layer. The machine-side layer realizes wind energy conversion, the DC-link/storage layer maintains DC bus voltage stability and provides power compensation, and the grid-side layer performs adaptive VSG-based frequency support.

As shown in Fig. 2, the grid frequency deviation and its rate of change are used as the inputs of the fuzzy logic controller to adjust the virtual inertia J online. Meanwhile, the damping coefficient D is optimized offline by PSO and applied to the VSG controller during real-time operation. The VSG controller generates voltage and current references, which are converted into PWM signals for the grid-side inverter. In this way, the adaptive VSG serves as the interface between the DC-side energy storage unit and the AC grid frequency, enabling the storage unit to compensate for wind power fluctuations and support grid frequency stability.

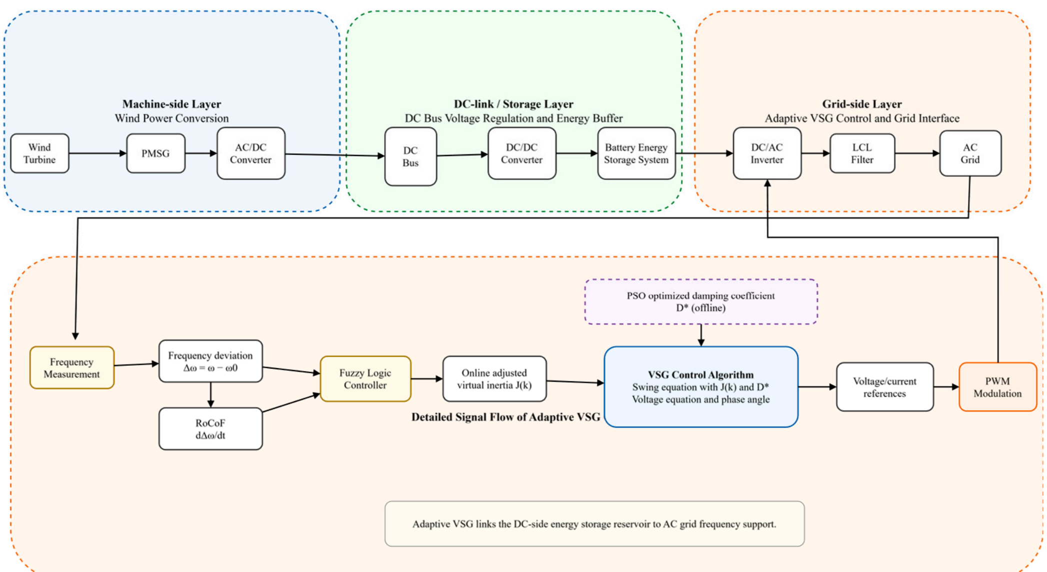

Figure 2: Signal flow of the adaptive VSG-based wind-storage combined system.

3 System-Level Modules and Their Control

3.1 Vector Control of the Machine-Side Converter

The steady-state mathematical model of PMSG in the dq rotating coordinate system is expressed as follows:

$$\begin{cases} u_{sq} = R_s i_{sq} + \omega L_d i_{sd} + \omega_r \psi_r \\ u_{sd} = R_s i_{sd} - \omega L_q i_{sq} \end{cases} \tag{1}$$

where R_s denotes the stator resistance; i_{sd} and i_{sq} represent the d-axis and q-axis stator current components, respectively; ω_r is the rotor angular velocity; L_d and L_q are the d-axis and q-axis stator inductances, respectively; and ψ_r stands for the rotor permanent magnet flux linkage.

The electromagnetic torque equation of the PMSG is given by:

$$T_e = \frac{3}{2} n_p i_{sq} \left[(L_q - L_d) i_{sd} + \psi_r \right] \tag{2}$$

where n_p is the number of pole pairs of the generator.

To eliminate the coupling between the d-axis and q-axis components in Eq. (1), feedforward decoupling control is adopted, and the control law of the current inner loop is derived as:

$$\begin{cases} u_{sd} = -\omega L_q i_{sq} + \left(k_p + \frac{k_i}{s}\right)(i_{sd}^* - i_{sd}) \\ u_{sq} = \omega L_d i_{sd} + \omega_r \varphi_r + \left(k_p + \frac{k_i}{s}\right)(i_{sq}^* - i_{sq}) \end{cases} \tag{3}$$

where k_p and k_i are the proportional coefficient and integral coefficient of the current inner-loop PI regulator, respectively.

For surface-mounted PMSG, the d-axis and q-axis inductances are approximately equal. By setting the d-axis current reference $i_{sd} = 0$, the electromagnetic torque Eq. (2) can be simplified to:

$$T_e = \frac{3}{2} n_p i_{sq} \psi_r \tag{4}$$

The q-axis current reference i_{sq} is generated by the DC bus voltage outer-loop PI regulator to maintain the stability of the DC bus voltage. Combining the feedforward decoupling control law Eq. (3) and the simplified torque Eq. (4), the vector control block diagram of the machine-side converter is illustrated in Fig. 3.

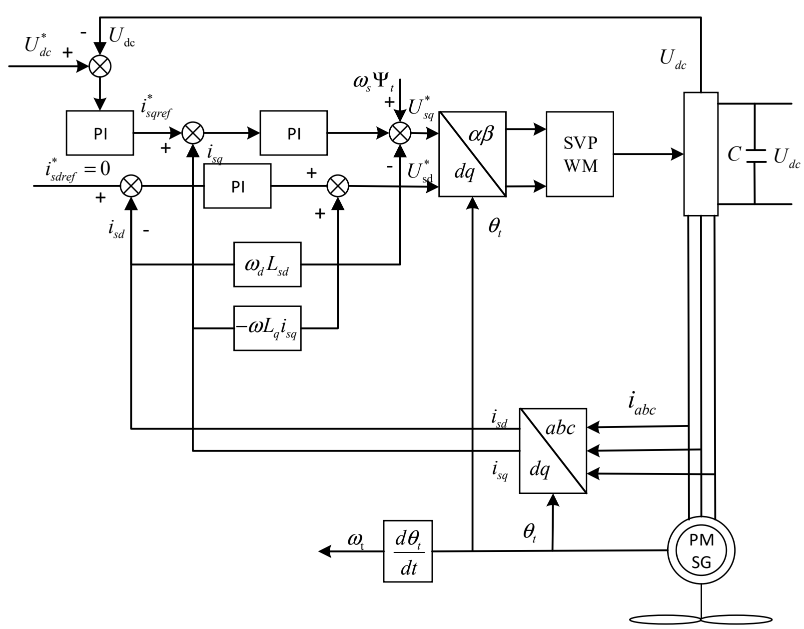

Figure 3: Control structure diagram of the machine-side converter.

3.2 VSG Control of the Grid-Side Converter

The overall control block diagram of VSG is illustrated in Fig. 4. Drawing on the second-order dynamic model of traditional synchronous generators, the rotor motion equation of the VSG is constructed to characterize its virtual rotor inertia and damping characteristics, as expressed in Eq. (5). Additionally, to enhance the stability of the active power-frequency (P-f) and reactive power-voltage (Q-V) control loops, two first-order low-pass filters are introduced in this paper to suppress fluctuations in instantaneous power, thereby improving the robustness of the control system.

$$\begin{cases} J\frac{d\omega}{dt} = \frac{P_m - P_e}{\omega_n} - D(\omega - \omega_n) \\ \frac{d\delta}{dt} = \omega \\ P_m = P_{\mathrm{ref}} + R_N(\omega_n - \omega) \\ U_{\mathrm{ref}} = U_N + R_V(Q_{\mathrm{ref}} - Q) \end{cases} \tag{5}$$

where J denotes the virtual moment of inertia; ω is the output angular velocity of the VSG; D represents the virtual damping coefficient; ω_n stands for the rated angular velocity of the power grid; δ is the power angle between the VSG output voltage and the grid voltage; R_N is the active power droop coefficient; R_V is the reactive power droop coefficient; P_{ref} is the reference value of the active power output by the VSG; U_{ref} is the rated amplitude of the VSG output voltage; U_N is the rated grid voltage; Q_{ref} is the reference value of the reactive power output by the VSG; Q is the actual reactive power.

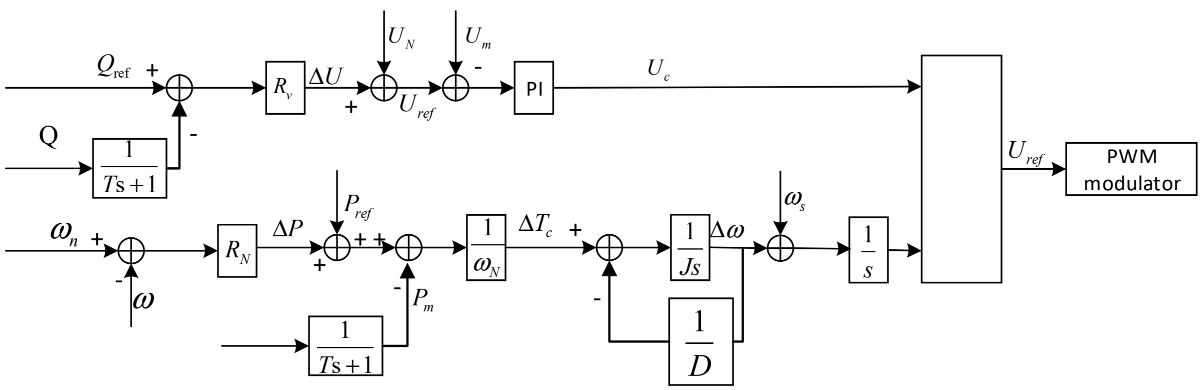

Figure 4: Control block diagram of virtual synchronous generator.

4 Stability Analysis of VSG

The grid-connected equivalent circuit of VSG is illustrated in Fig. 5. Taking the grid-connected bus voltage as the reference, the bus voltage is denoted as $U\angle 0$ and the VSG output voltage as $E\angle\delta$; $Z\angle\alpha$ represents the system transmission impedance, which equals the sum of the equivalent output impedance and the transmission line impedance, where $Z\angle\alpha = R + jX$, R is the equivalent resistance component, and X is the equivalent reactance component; δ is the power angle of the VSG, characterizing the phase angle difference between the output voltage vector of the grid-connected inverter and the grid voltage vector—specifically, the phase angle difference between the bridge arm midpoint voltage and the terminal voltage. It is the integral of the difference between the VSG virtual rotor angular velocity ω and the terminal angular velocity ω_c; I denotes the grid-connected output current.

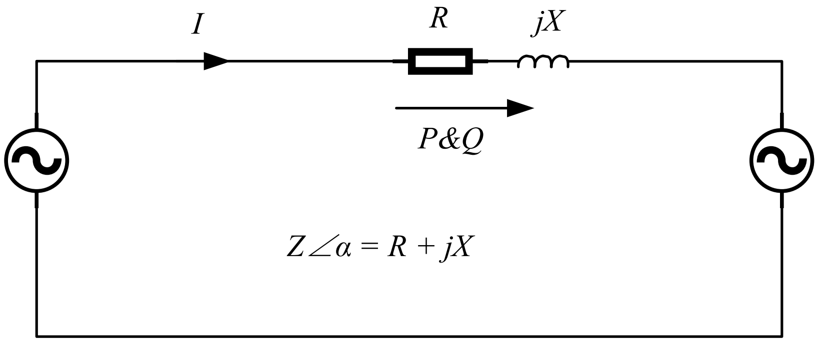

Figure 5: Equivalent circuit diagram of VSG grid connection.

For the actual grid-connected inverters of wind turbines, considering their large transmission power and the inductive nature of the system impedance, the system resistance can be neglected, i.e., $R \approx 0$. Accordingly, the equivalent system transmission impedance simplifies to $Z = jX$. When the VSG operates in a steady state, the phase angle difference between the inverter output voltage and the grid voltage is small (approaching 0), and the active power and reactive power exchanged between the VSG and the grid can be expressed as follows:

$$P = \frac{EU}{X} \sin \delta \tag{6}$$

$$Q = \frac{EU}{X} \cos \delta - \frac{U^2}{X} \tag{7}$$

With the grid-connected voltage kept constant, the control block diagram for active power-frequency regulation can be derived, as shown in Fig. 6. The small-signal closed-loop transfer function of the VSG's active power output under grid-connected operation is given by:

$$G(s) = \frac{EU}{JX\omega_n s^2 + DX\omega_n s + EU} = \frac{\frac{EU}{JX\omega_n}}{s^2 + \frac{D}{J}s + \frac{EU}{JX\omega_n}} \tag{8}$$

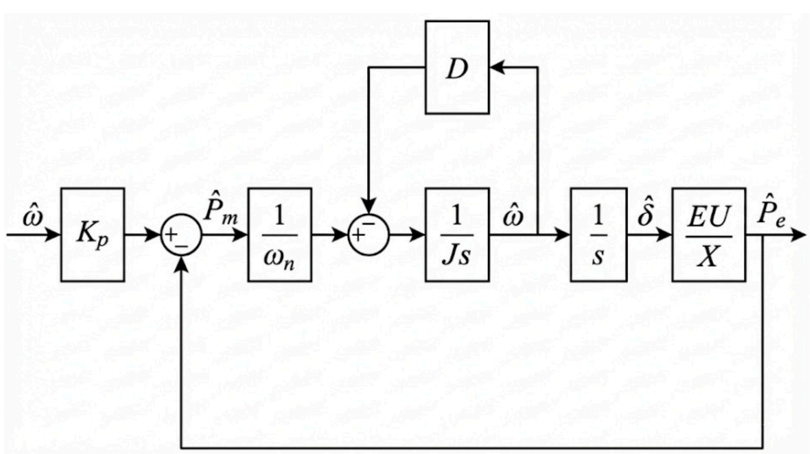

Figure 6: Small-signal model of VSG active power control.

The undamped natural oscillation angular frequency and damping ratio of the second-order system model are given by:

$$\begin{cases} \omega_0 = \sqrt{\frac{EU}{JX\omega_n}} \\ \xi = \frac{D}{2}\sqrt{\frac{X\omega_n}{JEU}} \end{cases} \tag{9}$$

Based on the second-order system theory, to ensure that the system exhibits satisfactory dynamic response performance, this paper analyzes the system under the underdamped condition, i.e., $0 < \xi < 1$, with an allowable error tolerance of 0.05. Accordingly, the settling time t_s and overshoot σ of the VSG control system can be expressed as:

$$\begin{cases} \sigma = \exp\left(-\frac{\xi\pi}{\sqrt{1-\xi^2}}\right) \times 100\% \\ t_s = \frac{3}{\xi\omega_n} \approx \frac{6J}{D} \quad (\Delta = 0.05) \end{cases} \tag{10}$$

From the above analysis, it can be concluded that the transient performance of the VSG system is jointly determined by the inertia coefficient J and the damping coefficient D. According to Eq. (10), when D is fixed, a larger J leads to a smaller damping ratio, larger overshoot, and longer settling time. Conversely, when J is fixed, a larger D results in a larger damping ratio, smaller overshoot, and shorter settling time. The following conclusions can be drawn: the dynamic performance of the VSG is dominated by the two parameters J and D. The inertia coefficient J mainly affects the oscillation frequency of the active power response, while the damping coefficient D mainly determines the decay rate of the active power oscillation.

The stability of the VSG is further investigated using the root locus method. The root locus diagrams of the system under different values of J and D are illustrated in Fig. 7. To guarantee stable operation of the system, the value of J is set to 0.5 under steady-state conditions in this paper.

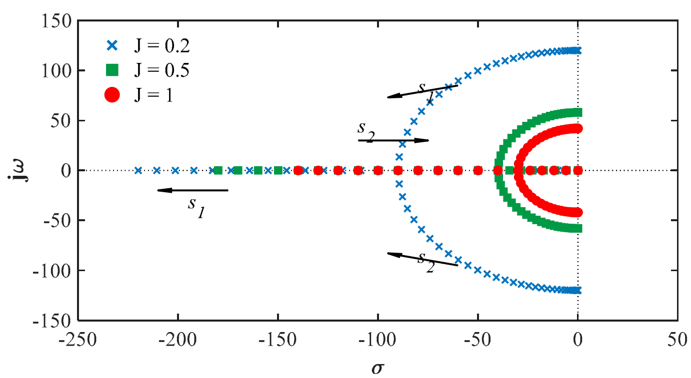

Figure 7: Root locus diagram of VSG parameters for different values of J and D.

5 VSG Parameter Adjustment Strategy

Although VSG technology effectively emulates the inertia and damping characteristics of synchronous generators, the conventional fixed-parameter control strategy can hardly satisfy the dynamic performance requirements of the system under different transient operating stages. By analyzing the angular velocity oscillation curve of the wind power VSG depicted in Fig. 8, it can be observed that in the intervals $[t_1, t_2]$ and $[t_3, t_4]$ the rate of change of frequency is relatively large and the frequency deviation continues to increase. In this case, a larger virtual inertia J is required to provide sufficient inertial support and suppress further frequency degradation. In contrast, during the intervals $[t_2, t_3]$ and $[t_4, t_5]$ the system is in the dynamic recovery stage. At this time, the virtual inertia J should be properly reduced to weaken the inertia lag effect, avoid excessive power overshoot, and accelerate the convergence to steady state.

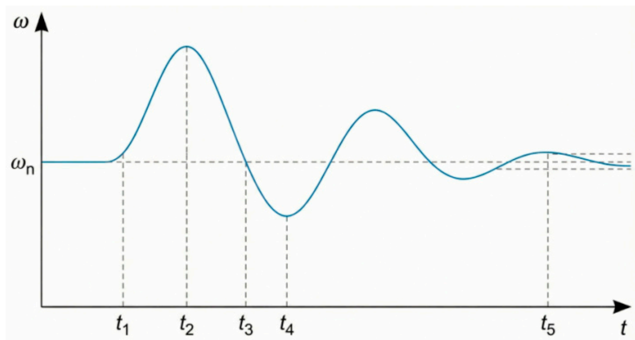

Figure 8: Angular velocity oscillation curve.

To address the above contradictions, this paper proposes a coordinated control strategy based on fuzzy logic for online adaptive adjustment of virtual inertia J and offline optimization of damping coefficient D via particle swarm optimization (PSO). For virtual inertia J, the strong nonlinear mapping ability and model-free characteristic of fuzzy logic are utilized to convert frequency oscillation characteristics into inference rules, thereby realizing real-time parameter tracking during the transient process and effectively reconciling the contradiction between fast disturbance suppression and stable recovery. Meanwhile, considering the strong coupling between damping coefficient D and J as well as its dominant effect on steady-state convergence, the PSO algorithm is adopted to globally search for the optimal fixed value of D that matches the fuzzy controller, so as to avoid control divergence caused by dual-parameter adaptive variation. The design of the fuzzy controller and the PSO optimization procedure are detailed in the following sections.

5.1 Fuzzy Logic-Based Adaptive Virtual Inertia Control

Traditional control methods rely on accurate mathematical models of the controlled object, but their control effectiveness is limited when dealing with complex and nonlinear systems. In contrast, fuzzy control can more flexibly cope with system disturbances and dynamic changes through fuzzy rules and logical reasoning, thus achieving more precise control performance. A VSG fuzzy controller is designed in this paper, as illustrated in Fig. 9, which adaptively adjusts the VSG inertia coefficient J in real time according to the real-time variations of angular frequency deviation $\Delta\omega$ and angular frequency change rate $d\omega/dt$.

The steps for formulating the fuzzy control rules are as follows: First, the angular frequency deviation and angular frequency change rate signals are fuzzified using quantization factors k_e and k_{ec}, respectively. Then, the pre-defined fuzzy control rules are applied for logical reasoning, and the reasoning result is defuzzified via a proportional factor k_u to obtain the variation value of the inertia coefficient. Finally, the variation value ΔJ is added to the initial inertia coefficient J_0 to obtain the real-time values of the inertia coefficient and damping coefficient during the transient period.

The definition of the fuzzy rules is as follows: The fuzzy subsets of the input and output variables are uniformly defined as {NB, NS, ZO, PS, PB}. The corresponding fuzzy control rules are given in Table 1. The quantization factors are taken as $k_e = 10$ and $k_{ec} = 0.3$, respectively, and the proportional factor is set to $k_J = 0.067$.

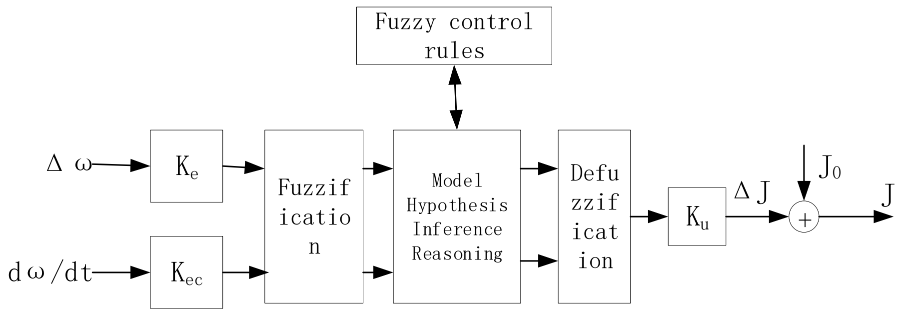

Figure 9: Structure diagram of fuzzy controller.

Table 1: Fuzzy control rule table.

ΔJ		Δω				
		NB	**NS**	**ZO**	**PS**	**PB**
$\frac{d\omega}{dt}$	NB	PB	PB	PB	ZO	NS
	NS	PB	PB	PS	NS	NB
	ZO	NB	NB	ZO	NB	NB
	PS	NB	NS	PS	PB	PB
	PB	NS	ZO	PB	PB	PB

5.2 PSO-Based Damping Coefficient Optimization

As stated previously, the damping coefficient D plays a critical role in system steady-state convergence and oscillation suppression. To match the fuzzy adaptive virtual inertia J designed in Section 5.1 and avoid control divergence caused by simultaneous time-variation of both parameters, the particle swarm optimization (PSO) algorithm is adopted in this paper to perform offline optimization of the damping coefficient D.

The optimization objective is to minimize the frequency deviation and achieve the shortest settling time under system disturbances. Therefore, the integral of time-weighted absolute error (*ITAE*) is selected as the fitness function (objective function). The *ITAE* performance index provides a good balance between the system dynamic response and steady-state error, and its expression is given as follows:

$$F_{ITAE} = \int_0^T t \cdot |\Delta\omega(t)| dt \tag{11}$$

In the expression, T denotes the total simulation time, and $\Delta\omega(t)$ represents the angular frequency deviation at time t. The smaller the value of the fitness function, the smaller the frequency overshoot and the faster the convergence speed of the system, which reflects a better control performance.

The PSO algorithm is inspired by the foraging behavior of bird flocks, and achieves global optimal search through cooperation and information sharing among individuals in the population. In the proposed strategy, the one-dimensional position coordinate of each particle corresponds to the value of the damping coefficient D. Assuming that the size of the particle swarm is N, the position of the i-th particle is denoted as x_i (i.e., D_i), and the candidate value of damping coefficient D, and the velocity is denoted as v_i. In each iteration, each particle updates its state by tracking two extreme values: one is the optimal solution found by the particle itself (individual extreme value, *pbest*), and the other is the optimal solution obtained by the entire population so far (global extreme value, *gbest*). The update formulas for the velocity and position of the particles are given as follows:

$$v_i^{k+1} = wv_i^k + c_1 r_1 (pbest_i^k - x_i^k) + c_2 r_2 (gbest^k - x_i^k) \tag{12}$$

$$x_i^{k+1} = x_i^k + v_i^{k+1} \tag{13}$$

In the expressions, k denotes the current iteration number; w is the inertia weight that balances the global and local search abilities; c_1 and c_2 are the learning factors (acceleration constants); r_1 and r_2 are random numbers uniformly distributed in the interval [0, 1].

To improve the reproducibility of the PSO-based damping coefficient optimization, the main hyper-parameters are specified in this study. Since only the damping coefficient D is optimized, each particle is defined as a one-dimensional variable. The search range of D is set to [1, 50] according to the small-signal stability analysis, root locus results, and preliminary simulation tests. The population size is set to 20, and the maximum number of iterations is set to 25 to balance optimization accuracy and computational burden. The inertia weight w decreases linearly from 0.9 to 0.4 to balance global exploration and local exploitation. The learning coefficients c_1 and c_2 are both set to 2.0, and the maximum particle velocity is limited to 20% of the search range to avoid excessive position updates.

During the optimization process, the damping coefficient D corresponding to each particle is imported into the VSG simulation model with the fuzzy controller established in Section 5.1 to perform a complete dynamic response test, and the corresponding ITAE value is calculated as the fitness. The iteration continues until the termination criterion is satisfied (i.e., reaching the maximum number of iterations or the fitness threshold). Finally, the globally optimal damping coefficient D_{opt} is obtained. The overall procedure of VSG parameter optimization combining fuzzy adaptation and the PSO algorithm is illustrated in Fig. 10.

6 System Simulation and Analysis

To verify the superiority of the adaptive VSG control strategy proposed in this paper, a simulation model of the adaptive VSG-based permanent magnet direct-drive wind-storage system was established with reference to Fig. 1, and corresponding simulation tests were carried out. The detailed simulation parameters of the system are presented in Table 2.

Table 2: Main Simulation Parameters of the System.

Parameters	Value
DC bus voltage/V	760
Filter inductor/mH	10
Filter capacitor/μF	20
Rated frequency/Hz	50
Active power droop coefficient	0.002
Reactive power droop coefficient	0.0001
DC bus capacitor/μF	2000

6.1 Frequency Modulation Characteristics of the System during Load Variations

Under the condition of constant wind speed and power command, the initial load is set to 20 kW. At t = 0.5 s, the system disconnects 10 kW of load, and at t = 1.0 s, 15 kW of load is reconnected. The reference active power is set to 25 kW, and the total simulation duration is 1.5 s. The simulation waveforms are illustrated in Fig. 11.

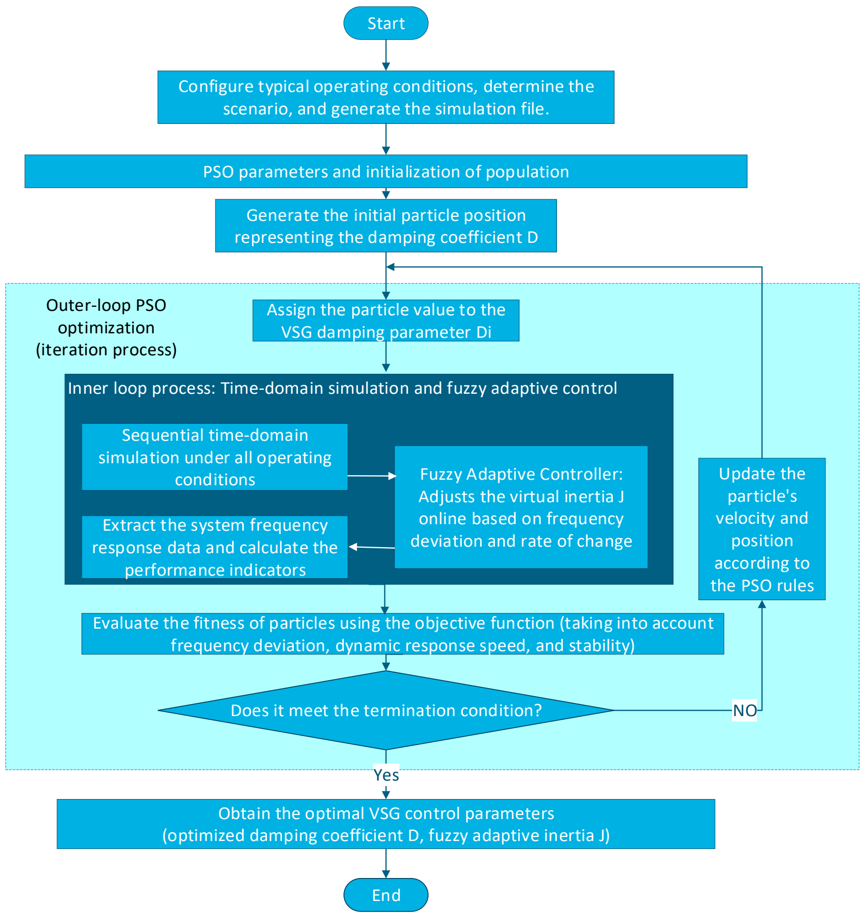

Figure 10: Flowchart of VSG parameter optimization based on fuzzy adaptation and PSO algorithm.

As shown in Fig. 11a, when the load decreases at t = 0.5 s, the generated active power temporarily exceeds the load demand, resulting in a transient frequency rise. When the load increases at t = 1.0 s, a transient active power deficit occurs, leading to a frequency drop. Compared with the fixed-parameter VSG control strategy, both the PSO-based co-optimized VSG and the GWO-based co-optimized VSG can effectively suppress the frequency fluctuation caused by load disturbances and improve the frequency recovery process.

It can be observed from the frequency response curves that the fixed-parameter VSG produces a larger frequency deviation during load variations, indicating that a fixed damping coefficient is difficult to adapt to different disturbance conditions. In contrast, after the damping coefficient is optimized by intelligent optimization algorithms, the VSG controller can obtain more suitable damping characteristics, thereby improving the active frequency support capability of the wind-storage combined system. The PSO-based co-optimized VSG and the GWO-based co-optimized VSG both show favorable frequency regulation performance under the same ITAE objective function and damping coefficient search range, which verifies the effectiveness of optimization-based damping coefficient design in improving transient frequency stability.

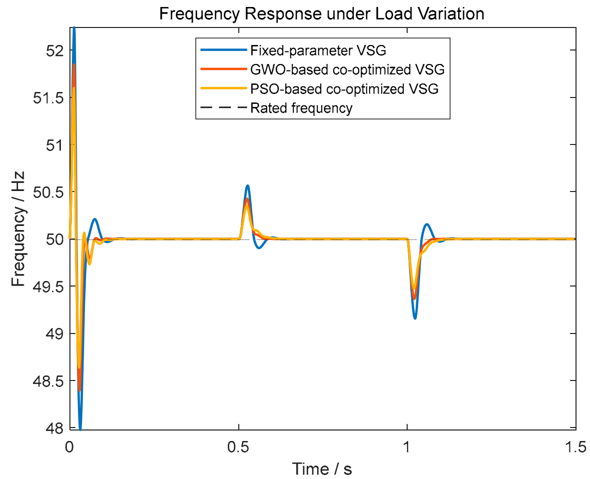

(**a**) Frequency response curve

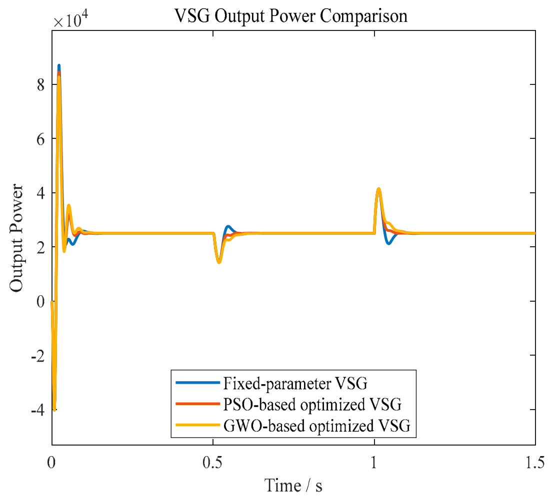

(**b**) Output power of VSG

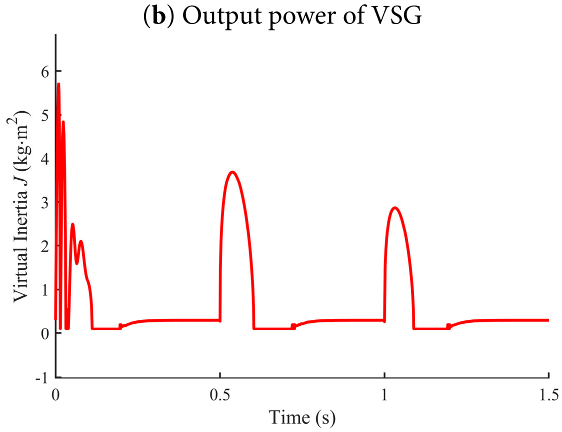

(**c**) Adaptive rotational inertia

Figure 11: Frequency regulation characteristics under load variation.

To further quantitatively evaluate the frequency regulation performance of different control strategies, the key dynamic indices of the fixed-parameter VSG, PSO-based co-optimized VSG, and GWO-based co-optimized VSG under load variation are summarized in Table 3.

Table 3: Frequency regulation performance comparison under load variation.

Control Strategy	Frequency Nadir/Hz	Frequency Peak/Hz	Maximum Frequency Deviation/Hz
Fixed-parameter VSG	49.16	50.16	0.84
GWO-based co-optimized VSG	49.37	50.43	0.63
PSO-based co-optimized VSG	49.48	50.39	0.52

6.2 Frequency Modulation Characteristics of the System under Wind Speed Variations

Under the condition of constant system load and power command, the initial active power reference is set to 20 kW, with the load fixed at 30 kW. The wind speed profile is defined as W = [8, 12, 10] m/s, corresponding to time instants t = [0, 0.5, 1.0] s. The total simulation duration is 1.5 s, and the simulation waveforms are illustrated in Fig. 12.

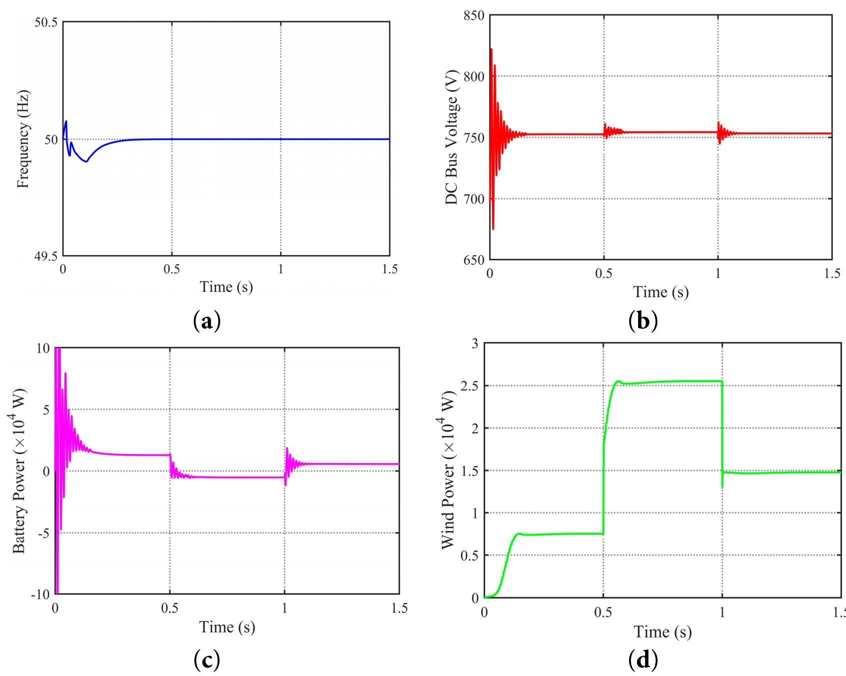

Figure 12: System simulation waveforms under varying wind speeds. (**a**) Frequency-response curve; (**b**) DC bus voltage; (**c**) Energy storage battery output power; (**d**) Output power of the wind turbine.

As depicted in Fig. 12a, after the system starts and reaches steady state, the system frequency remains stable at 50 Hz. Despite the step changes in wind speed at t = 0.5 s and t = 1.0 s, the system frequency maintains stability with no obvious fluctuations.

Fig. 12b illustrates the disturbance rejection capability of the DC bus voltage. At the moment of wind speed step change, the DC bus voltage exhibits a brief fluctuation. However, under the fast regulation of the DC-side controller, the voltage fluctuation amplitude is limited within a reasonable range and quickly returns to the rated value, providing stable energy support for the VSG inverter.

Fig. 12c,d visually demonstrates the power complementarity between the wind turbine and the energy storage unit. During the interval 0–0.5 s, the wind speed is low, resulting in insufficient wind turbine output to meet the 20 kW grid-connected power command. In this case, the energy storage unit operates in discharge mode to compensate for the power deficit. At t = 0.5 s, the wind speed increases to 12 m/s, and the wind turbine output rises significantly and exceeds the grid demand. Consequently, the energy storage unit rapidly switches from discharge to charge mode to absorb the surplus wind power, thereby achieving power supply-demand balance. After t = 1.0 s, as the wind speed decreases, the energy storage unit adjusts its output again, maintaining a complementary "mutual increase and decrease" relationship with the wind turbine power.

Based on the above analysis, under wind speed fluctuation conditions, the energy storage unit rapidly absorbs and releases power to smooth the randomness of wind energy. The proposed strategy not only ensures the stability of the DC bus voltage but also enables the grid-side VSG to output constant active power, verifying the stable operation capability of the wind-storage integrated system under source-side disturbances.

6.3 Sensitivity and Robustness Discussion

Based on the small-signal model and root locus analysis in Section 4, the effects of key VSG parameters on system performance can be further discussed. The virtual inertia J mainly affects the initial inertial response and the rate of frequency change. A larger J can enhance inertial support and reduce the frequency change rate, but it may slow down the recovery process. In contrast, a smaller J can improve the response speed, but may lead to larger frequency fluctuations under sudden disturbances. The damping coefficient D mainly affects oscillation suppression and steady-state convergence. If D is too small, the system damping is insufficient and frequency oscillations may increase. If D is too large, the system may become over-damped, resulting in a slower dynamic response. Therefore, the proposed strategy adopts fuzzy logic to adjust J online and uses PSO to optimize D offline, so as to balance inertial support, oscillation suppression, and recovery speed. In addition, since the damping coefficient is a one-dimensional decision variable and its search range is constrained by the stability analysis, moderate changes in PSO hyper-parameters mainly affect the convergence speed rather than the basic stability of the optimized VSG system. The comparison with the GWO-based strategy also indicates that the optimization-based damping design can maintain effective frequency regulation performance under the same disturbance condition.

6.4 Practical Implementation Considerations

Although the proposed adaptive VSG strategy has been verified through MATLAB/Simulink simulations, several practical issues should be considered before engineering application. The frequency support capability of the energy storage unit is constrained by its rated power, capacity, SOC range, charge-discharge efficiency, and battery aging. Therefore, the VSG power command should be coordinated with SOC management and battery protection limits. In addition, frequency measurement, signal filtering, controller calculation, and PWM generation may introduce delays, which could affect the dynamic adjustment of virtual inertia. Grid uncertainties, such as impedance variation, load fluctuation, and renewable power volatility, may also influence the frequency support performance. Since the proposed method adjusts only the virtual inertia online while the damping coefficient is optimized offline, the online computational burden is relatively low and suitable for real-time implementation. Future work will focus on hardware-in-the-loop tests and experimental verification under practical operating constraints.

7 Conclusion

To address the reduced system inertia and degraded frequency stability caused by high renewable energy penetration, this paper proposes a hierarchical coordinated VSG control strategy for a wind-storage combined grid-connected system with DC-side energy storage. In the proposed strategy, fuzzy logic is used for online adaptive virtual inertia regulation, while PSO is employed for offline damping coefficient optimization. This online-offline coordinated design improves transient inertial support and oscillation damping while reducing the coupling risk between virtual inertia and damping coefficient.

Simulation results show that the proposed PSO-based co-optimized VSG strategy effectively suppresses frequency fluctuations under load disturbances. Compared with the fixed-parameter VSG and the GWO-based co-optimized VSG strategy, the proposed method achieves smaller maximum frequency deviation and better dynamic recovery performance. Under wind speed variations, the energy storage unit can rapidly compensate for wind power fluctuations, maintain DC bus voltage stability, and ensure stable active power output. Therefore, the proposed strategy enhances the active frequency support capability and operational stability of the wind-storage integrated system.

In addition, the proposed strategy has practical significance for improving active frequency support in wind-storage combined systems under high renewable energy penetration. Future work will focus on hardware-in-the-loop validation, experimental verification, and further evaluation under practical operating conditions, including communication delay, battery aging, and grid uncertainty, so as to promote its engineering deployment in renewable-dominated power systems.

Acknowledgement: This research was supported by the Science and Technology Project of State Grid Shanghai Electric Power Company (No. 52090R250007): Research on Multi-Objective Optimization Control and Risk Prevention Technology for Far-reaching Offshore Wind Turbines and Clusters Driven by Multi-Source Heterogeneous Data.

Funding Statement: The authors received no specific funding for this study.

Author Contributions: All authors contributed to the idea and control design of the study. Ruanming Huang: Methodology, Software, Investigation, Writing. Yuchen Qi: Methodology, Software, Writing. Yaoliang Zhu: Methodology, Resources, Funding Acquisition. Chen Qian: Software, Resources, Funding Acquisition. Haojie Li: Methodology, Software, Writing. Bing Wang: Methodology, Investigation, Supervision. All authors reviewed and approved the final version of the manuscript.

Availability of Data and Materials: Data available within the article.

Ethics Approval: Not applicable.

Conflicts of Interest: The authors declare no conflicts of interest.

References

1. Kroposki B, Johnson B, Zhang Y, Gevorgian V, Denholm P, Hodge BM, et al. Achieving a 100% renewable grid: operating electric power systems with extremely high levels of variable renewable energy. IEEE Power Energy Mag. 2017;15(2):61–73. [CrossRef].
2. Dreidy M, Mokhlis H, Mekhilef S. Inertia response and frequency control techniques for renewable energy sources: a review. Renew Sustain Energy Rev. 2017;69:144–55. [CrossRef].
3. Fang J, Li H, Tang Y, Blaabjerg F. On the inertia of future more-electronics power systems. IEEE J Emerg Sel Top Power Electron. 2019;7(4):2130–46. [CrossRef].
4. Zhong QC, Weiss G. Synchronverters: inverters that mimic synchronous generators. IEEE Trans Ind Electron. 2011;58(4):1259–67. [CrossRef].
5. Arani MFM, El-Saadany EF. Implementing virtual inertia in DFIG-based wind power generation. IEEE Trans Power Syst. 2013;28(2):1373–84. [CrossRef].
6. Shadoul M, Ahshan R, AlAbri RS, Al-Badi A, Albadi M, Jamil M. A comprehensive review on a virtual-synchronous generator: topologies, control orders and techniques, energy storages, and applications. Energies. 2022;15(22):8406. [CrossRef].

7. Shi T, Sun J, Han X, Tang C. Research on adaptive optimal control strategy of virtual synchronous generator inertia and damping parameters. IET Power Electron. 2024;17(1):121–33. [CrossRef].
8. Zhao J, Lyu X, Fu Y, Hu X, Li F. Coordinated microgrid frequency regulation based on DFIG variable coefficient using virtual inertia and primary frequency control. IEEE Trans Energy Convers. 2016;31(3):833–45. [CrossRef].
9. Thomas V, Kumaravel S, Ashok S. Fuzzy controller-based self-adaptive virtual synchronous machine for microgrid application. IEEE Trans Energy Convers. 2021;36(3):2427–37. [CrossRef].
10. Hou X, Sun Y, Zhang X, Lu J, Wang P, Guerrero JM. Improvement of frequency regulation in VSG-based AC microgrid via adaptive virtual inertia. IEEE Trans Power Electron. 2019;35(2):1589–602. [CrossRef].
11. Pournazarian B, Sangrody R, Lehtonen M, Gharehpetian GB, Pouresmaeil E. Simultaneous optimization of virtual synchronous generators parameters and virtual impedances in islanded microgrids. IEEE Trans Smart Grid. 2022;13(6):4202–17. [CrossRef].
12. Coello CAC, Pulido GT, Lechuga MS. Handling multiple objectives with particle swarm optimization. IEEE Trans Evol Comput. 2004;8(3):256–79. [CrossRef].
13. Coello Coello CA, Reyes-Sierra M. Multi-objective particle swarm optimizers: a survey of the state-of-the-art. Int J Comput Intell Res. 2006;2(3):287–308. [CrossRef].
14. Altawallbeh A, Alassi A, Meskin N, Al-Hitmi MA, Massoud AM. Small-signal stability analysis and parameters optimization of virtual synchronous generator for low-inertia power system. IEEE Access. 2025;13:107227–43. [CrossRef].
15. Gurski E, Kuiava R, Perez F, Benedito RAS, Damm G. A novel VSG with adaptive virtual inertia and adaptive damping coefficient to improve transient frequency response of microgrids. Energies. 2024;17(17):4370. [CrossRef].
16. Zhang X, Shao Z, Fu Y, Cao Y. Frequency safety demand and coordinated control strategy for power system with wind power and energy storage. IET Gener Transm Distrib. 2025;19(1):e70018. [CrossRef].
17. Jiang Y, Wang C, Xiao L, Yu D, Zhang X. Wind/storage coordinated control strategy based on system frequency regulation demands. Energy Rep. 2024;11:1551–9. [CrossRef].
18. Zhang X, Cao Y, Li H, Liu Y. Multi-stage virtual angular frequency control of wind-storage generation system for frequency warning requirements. IET Renew Power Gener. 2025;19:e70118. [CrossRef].
19. Qi X, Lei L, Yu C, Ma Z, Qu T, Du M, et al. Adaptive distributed MPC based load frequency control with dynamic virtual inertia of offshore wind farms. IET Control Theory Appl. 2024;18(17):2228–38. [CrossRef].
20. Hu J, Wen W, Li Y, Liu X, Guo J. A multi-timescale characteristics analysis of the network power response excited by voltage with time-varying amplitude and frequency. Engineering. 2025;51:49–61. [CrossRef].
21. Assogna R, Ciabattoni L, Comodi G. PSO-based supervisory adaptive controller for BESS-VSG frequency regulation under high PV penetration. Energies. 2025;18(20):5401. [CrossRef].
22. Parsa SM. Physics-informed machine learning meets renewable energy systems: a review of advances, challenges, guidelines, and future outlooks. Appl Energy. 2025;402:126925. [CrossRef].
23. Neshat M, Sergiienko NY, Rafiee A, Mirjalili S, Gandomi AH, Boland J. Meta wave learner: Predicting wave farms power output using effective meta-learner deep gradient boosting model: A case study from australian coasts. Energy. 2024;304:132122. [CrossRef].
24. Li S, Cao P, Li X. Optimization method of energy storage system based on improved VSG control algorithm. J Energy Storage. 2024;101:113041. [CrossRef].